Variability of the stress pattern in the continental margin of Egypt

Asem Salama[1], Mohamed EL Gabry[1], Hesham Hussein [1], Mona Abdelazim[1]

1 **National Research Institute of Astronomy and Geophysics (NRIAG), 11421 Helwan, Cairo, Egypt.**

Corresponding author: asem.mosatafa@nriag.sci.eg

Key points:

1. Focal mechanism calculated using HASH software give A quality for the recent earthquakes events, B and E quality for past margin events.
2. The stress pattern derived from borehole breakout measurements wasn't correlated with the identified stress axis on the Egyptian margin.
3. The mechanism and stresses change from pure reverse in the western part to strike-slip with some reverse component in central-eastern part.

Abstract

We have studied the focal mechanisms of eleven earthquakes with magnitudes of $M_{L \geq} 3.8$ on the continental margin of Egypt and the adjacent onshore region from 1951 to 2020 to identify the stress regime and its spatial variations. The uncertainty parameters of each solution are evaluated using HASH software. The stress pattern obtained from focal solutions in the western province matches a compressional stress field with an NNW-SSE orientated compression axis, which corresponds to the direction of movement of the Nubia plate relative to Eurasia. On the other hand, the stress pattern derived from drilling-induced fractures and borehole breakout measurements is not correlated with the identified stress axis. The focal solutions of the recent earthquakes in the eastern-central province of the Nile Deep-Sea Fan indicate the strike-slip stress regime is the prevailing mode of deformation with an almost horizontal ESE-WSW compression axis and an almost horizontal N-S extension axis. Two responsive conjugate strike-slip faults that include both sinistral and dextral faults accommodate this strike-slip deformation style. The stress regime existing in the eastern-central province directly contradicts the northward convergent of the Nubian-Anatolia plates along the Cypriot arc. The stress pattern deflection in the eastern-central province of the Nile Deep-Sea Fan may be attributed to kinematic adaptation resulting from the deformation in and around the Eratosthenes Seamount rigid block as it impinges on the central part of the Cypriot arc. Toward the Egyptian onshore, the extension pattern was behaving differently from the compression stress pattern of the offshore continental margin.

Keywords: Seismicity and tectonics, Egyptian continental margin, present-day stress pattern, Nile Deep-sea Fan, Focal mechanism.

Summary

FOCMEC; HASH and PINV software are used to invert the polarity data for eleven earthquakes to get the optimum focal mechanism solutions of $M_{L \geq} 3.8$ from 1951 to 2020 on Egypt continental margin with calculating the uncertainties. The data was obtained from the

Egyptian National Seismological Network and International Data Center of the comprehensive Test Ban Treaty Organization (CTBTO) in addition to the available polarities in the International Seismological Center (ISC). We used two different velocity models; Western Deseret (WD) and Mediterranean (MC), which cover a variety of possible structures for the study area (Marzouk & Makris, 1979). We have defined the main deformation features, which occurred by, correlated the stresses obtained from focal mechanism data with structural, boreholes and GPS studies. These are a reverse faulting mechanism with some strike-slip motion in the western province zone of the Nile Deep-Sea Fan shows margin perpendicular NNW-SSE compression direction. In the central-eastern province, the sinistral and dextral faults accommodate this strike-slip deformation style of the NE-SW trending Rosetta-Qattara Fault Zone and the NW-SE trending Misfaq-Bardawil Shear Zone. The extension pattern on the Egyptian onshore was behaving differently from the compression stress pattern of the offshore margin.

1. Introduction

Seismic activity occurring in the passive margin constitutes a low percentage compared to the activity along the plate boundaries**.** Johnston, 1989 evaluated the passive continental margin earthquakes worldwide in combination with tectonic features. The passive continental margins that were created under the intra-continental rifting extension are presently under compression. They represent significant locations for stable continental interiors earthquakes. The prevailing faults existing in the passive margins worldwide are strike-slip, thrust and a limited number of normal faults, suggesting the reversal of the originally created normal faults. Faults created during rifting continue as zones of weakness for a long period of time, even though the stress regime turns into compression. Such faults are known to be linked with the frequent stable continental interiors earthquakes. Globally, the 1906 Exmouth plateau (Australia) was the largest earthquake that occurred in the passive continental margin (M_s=7.8) (Hengesh and Whitney 2016).

The Egyptian passive continental margin manifested scattered activity with small and moderate magnitude earthquakes (Maamoun et al., 1984). Three significant earthquakes struck the margin during the period from 1900 to 2011. The largest recorded events in the margin include the Sep., 12, 1955 (M_L = 6.2) and May 28, 1998 (M_L =5.9) Alexandria offshore events in addition to January 30, 1951 (M_L= 5.6) Levantine basin event. From the histor0ical record, the two largest events struck the margin in 320 and 956 AD. Both earthquakes occurred to the north of the September 12, 1955 epicenter (M_L=6.2) (Korrat et al., 2005).

Tectonically, the Egyptian continental margin (Figure 1) is affected by the interaction among three tectonic plates (African, Arabian and Eurasian) and several micro-plates as Anatolian and Aegean. The deformation existing in this region is related to northward subduction of the African Plate and the north-northwest movement of the Arabian plate towards the Eurasian plate (Argus et al. 1989; Rosenbaum et al. 2002) and the westward pushing out of the Aegean–Anatolian micro-plate which is marked by the Anatolian fault zones both in the East and the North (Le Pichon et al. 1988; McClusky et al., 2000). The extracted GPS velocity vectors of the central and southern Aegean plates relative to Eurasia suggest an average movement of 33 mm/year towards the SW, while the Anatolian plate moves 21mm/year westward relative to Eurasia (Reilinger et al., 2006; Figure 1). All Egyptian sites are moving N to NNW relative to Eurasia with the same magnitude, 6.5 ± 1 mm/yr on the average except Sinai region, which moves 8.2 ± 0.8 mm/yr to N-NE direction (Saleh and Becker, 2015) as shown in Figure 1.

During the last 10 years, some earthquakes with moderate magnitudes have occurred in the Egyptian continental margin and adjacent onshore area, which includes October 19, 2012, January 17, 2013, September 3, 2015, May 15, 2019, July 5, 2019, and April 11, 2020 earthquakes with magnitudes M_L 4.8, 4.5, 4.3, 4.0, 4.1 and 3.8 calculated by ISC bulletin respectively. Previous studies of various authors using the different techniques suggested variable fault plane solutions of the October 19, 2012, and January 17, 2013, continental margin events. Badawy et al., 2015 suggested a normal dip-slip faulting mechanism with a

minor strike-slip component. Badreldin et al., 2018, on the other hand, showed that both earthquakes exhibited a strike-slip faulting mechanism with a minor reverse component while Hassoup et al., 2016 solution indicated a reverse faulting mechanism with a strike-slip component. The focal mechanism solutions of both events should be re-investigated as a result of this contradiction. Fortunately, a large number of stations, distributed in good azimuth coverage recorded the majority of the recent continental margin earthquakes. This will enable us to get more reliable focal mechanism solutions for the six most recent continental margin earthquakes. We have also reinvestigated the solutions of the previous earthquakes (Korrat et al., 2005). As these solutions are combined with the recent ones, a thorough comprehension of the stress state on the Egyptian continental margin will arise. Thanks a lot, to the digital seismological networks, which provided us with a lot of information that helps us to improve our results. These networks facilitate the recording of small magnitude earthquakes and the construction of extra focal mechanism solutions. The global stress pattern in the passive continental margins revealed dynamic interplays between local and regional stresses, as well as between stress domains and weakness zones, which, may lead to the reactivation of older fault zones under favourable conditions (e.g., Mandal et al., 1997).

The main target of this paper is to analyze the available focal mechanism solutions in the Egyptian continental margin as a way of understanding the spatial distribution of the present-day stress field. We used three software included in Seisan 2.5 (Havskov and Ottemöller, 2020), which are FOCMEC (Snoke et al., 1984), HASH (Hardebeck & Shearer, 2008) , PINV (Suetsugu, 1998) to investigate the largest events with $M_L \geq 3.8$ occurred on the Egyptian continental margin. The HASH technique enables us to determine the preferred fault planes for each event, allowing us to assess the quality of the solutions. Then, the stress field obtained in this area was then compared to that inferred from structural geology and the Egyptian GPS geodetic network. This research work is as an extension of Korrat et al., 2005 previous study.

2. Tectonic Setting

The Egyptian continental margin represents a wide variety of geodynamic elements (Figure 2) which encompass the Eastern Mediterranean Sea. These elements include the Suez Rift in the southeast, the Dead Sea –the Levant in the east, the East Anatolian Fault in the northeast, the Cyprian Arc and Hellenic Arc northward (Loncke et al., 2006). The continental margin of Egypt exists to the south of the Mediterranean ridge back to the Herodotus abyssal plain where the seafloor is dominated by the existence of Herodotus basin, Nile Deep-Sea Fan and Eratosthenes Seamount. It marks the zone of transition between the oceanic and continental crusts (Figure 2) where the stress field transitions from predominant extensional stress on the Egyptian territory to compressional stress along the Hellenic Arc convergence zone (experiencing north-south compression), as shown in various studies (Abu Elenean, 1997; Korrat et al., 2005; Abou Elenean and Hussein, 2007; Bosworth, 2008). The Nile Deep-Sea Fan is bounded to the east by the Dead Sea Transform zone and to the north by the convergent zone of Cyprus and the Mediterranean Ridge. The elevated thick Eratosthenes structure existing between the Nile cone and Cyprus interrupts the collision between Africa and Anatolia (Kempler, 1998). Three major morphological structural provinces in the east, central, and west, characterize the Nile Deep-Sea Fan.

The continental margin of Egypt took its present form through several tectonic movements during the period from Late Triassic to the Present (Table 1). The Early Mesozoic-Cenozoic tectonic phase is the Neo-Tethyan rifting phase that originated from the opening of the Neotethys and the divergent motion between Afro-Arabia and Eurasian plates. (Robertson and Dixon, 1984; Moustafa and Khalil, 1989, 1994; May, 1991; Argyriadis et al., 1980; Moustafa,2020). This tectonic phase started at the Late Triassic and ended in the Early Cretaceous. A second phase began in the Late Cretaceous and continued until recent time. This phase was characterized by the consecutive convergence of both African and Eurasian Plates which resulted in the closure of New-Tethys. Moustafa, 2020 demonstrated the impact of

these movements on northern Egypt, both offshore and onshore. The rifting phase contributed to the creation of the rift parallel NE-SW trending extensional basins boundary faults, reflecting NW-SE divergent motion. The NE-SW trending Rosetta-Qattara fault, which exists along the Nile cone's western border, may be one of these boundary faults (Abd El-Fattah et al., 2018). This fault which extends offshore through the western desert is a major NE-SW trending fault stretching for 160 Km and dipping to NNW. It marks the border of the Herodotus basin which is characterized by its oceanic to the sub-oceanic crust and restrained the Levant basin rifting field (Tassy et al., 2015). The Late Cretaceous (Late Santonian)-Tertiary compressional stress, affected the Rosetta-Qattara fault. The compression direction during this phase was NW or WNW (Eyal and Reches, 1983; Moustafa, 2020). This deformation phase was associated with the convergence between African and Eurasian Plates which gave rise to positive structural inversion. Onshore inverted structures indicated that this inversion may be formed by transpressive stress with a small dextral slip component, giving evidence that the direction of convergence may be WNW-ESE. The deformation associated with the continued plate convergence during Miocene and younger led to the generation of NE-SW trending hanging wall anticlines and reverse slip in the region between Rosetta-Qattara fault and Mediterranean Ridge which indicate SE compression direction (Moustafa, 2020). Rosetta--Qattara fault was reactivated as a left-lateral strike-slip fault due to the consecutive convergence of both African and Eurasian Plates at Pre-Tortonian (Pre Late Miocene) (Sheim et al., 2002) or Messinian (Late Miocene) (Abd El-Fattah et al., 2018). Hanafy et al., 2017 pointed out that the Rosetta-Qattara fault seemed to be active during the Early Miocene with right-lateral transpressive slip motion. In Pliocene Epoch and younger, Rosetta-Qattara fault reveals essentially normal dip-slip movement. The rifting phase led also to the formation of WNW-ESE trending transform fault which extends along the margin of NW Egypt and NE Libya (Tari et al., 2012). This fault defines a border between the offshore oceanic crust and gently expanding Egyptian continental crust (Moustafa, 2020).

The NNW trending Misfaq-Bardawil fault is another fault trend that is cutting across the eastern Nile Deep-Sea Fan province to the south of Eratosthenes Seamount and superimpose deeper basement fault (Mascle et al., 2001; Dolson et al., 2014). This fault is located under the area of the NW-SE trending detachment Oligocene-Miocene folds which exist in both central and eastern Nile Deep-Sea Fan. These folds formed as a result of the plate convergence in the Miocene and recent times. It reflects the NE- SW direction of shorting through the presence of reverse slip and the formation of hanging wall anticlines (Moustafa, 2020). This direction is different from the NW-SE dominant convergent direction of the Late Cretaceous-Early Tertiary. Moustafa, 2020 attributed such variation in the compressive stress direction to the local variation associated with the Eratosthenes Seamount in addition to detachment resulting from the existence of ductile units in the geological section. The Misfaq-Bardawil fault is believed to be a positively inverted Oligocene normal slip faults as confirmed by Dolson, 2014 and Hussein, 2013. In the Middle Miocene, Hanfy et al., 2017 suggested that the Misfaq-Bardawil fault was subjected to dextral movement. In the Late Miocene, the Misfaq-Bardawil trend was reactivated as an uplifted horst structure (Mosconi et al., 1996; Shaaban et al., 2006). In Pliocene, The Misfaq-Bardawil trend shows strike-slip tectonic activity which may be attributed to transtensive stress (Abdel Aal et al., 2001, El Barkooky and Helal.,2002). The sense of motion was interpreted as a right-lateral sense of motion (Abdel Aal et al., 2001) or left-lateral sense of motion (El Barkooky and Helal.,2002).

The present-day stress field measured from 588 breakouts data and 68 drilling-induced fractures offshore the Nile Delta indicated a typical margin parallel deltaic compressional stress axes trending NNE to SSW in the western province, E-W in the central province and ESE-WNW in the eastern province (Tingay et al., 2012). The preliminary results of the calculated deformation from the GPS data of the permanent Egyptian Network and the European Permanent Network in the Eastern Mediterranean Sea suggested mostly pure reverse faulting mechanism with a P-axis trending NNE-SSW in the western Nile Deep-Sea Fan Province with a smaller ellipse error (Zeman et al., 2010). The results of deformation in the Eastern provinces show a huge ellipse error. Therefore, it cannot be taken into account.

The Levant Basin is bordered to the East by the Levantine fault system that created a complicated geodynamic framework. The Levant basin is characterized by the existence of three main fault trends: ENE-WSW right-lateral strike-slip faults, NW-SE oriented normal faults and NE-SW trending reverse faults (Ghalayini et al., 2014). All of these fault trends were active in the first phase of the Levantine fault system movement (Freund et al., 1970; Garfunkel, 1981; Quennell, 1984). Only the ENE-WSW dextral strike-slip faults were active during the second phase of the Levantine fault system in the Pliocene to the present day. The continuous sinisterly movement along the Levantine fault system was the main factor for the continuation of the activity along with this fault trend. The manifestation of uniformly spaced NW-SE trending normal faults in the central part of the Levantine basin might not be created by this regional movement but rather to a local stress-field oscillation which affected only the Oligocene-Miocene (Ghalayini et al., 2014).

3. Seismicity of the Continental Margin

The spatial distribution of the Egyptian continental margin earthquakes, collected from the International Seismological Center and the Egyptian National Seismological Network (ENSN) bulletins for local magnitude M_L ranging from 3.8 to 6.2 and covering the years 1900 to 2020 is shown in Figure 3. The earthquake activity, which has been distributed across the margin is scattered. Over the last ten years, three significant earthquakes, including October 19, 2012, January 17, 2013, September 3, 2015 and July 5, 2019 events occurred along the NE trending Rosetta-Qattara fault zone, the associated sub-parallel faults and its onshore extension with local magnitudes M_L ranging from 3.8 to 4.8 calculated by the International Seismological Centre (ISC). This fault separates the western Nile Cone province from the central one. The September 3, 2015 took place along the Alamein fault which represents the extension of the Qattara –Rosetta fault. On May 15, 2019, an earthquake with magnitude M_L =4.0 occurred along with one of the sub-parallel faults to the NNW- SSE trending Misfaq-Bardawil main fault. This event represents the largest among the limited number of small

magnitude earthquakes which happened in the Misfaq- Bardawil fault zone. Three earthquakes with local magnitudes $M_L \geq 4.4$ have struck the western Nile cone province during the period from 1955 to1988. The largest documented earthquake in this province occurred on September 12, 1955. This earthquake has caused widespread damage in the Nile Delta between Cairo and Alexandria. In the province of Bahira, a maximum intensity of VII - VIII has been reported where five people have been killed and 61 injured. Three hundred older brick buildings have been destroyed on the western side of the Nile Delta. This earthquake has been also felt throughout the Eastern Mediterranean, in Palestine, Cyprus, Crete, the island of Dodencense and Athenes. A significant felt earthquake of local magnitude 5.9 (M_L) struck the continental shelf periphery on May 28, 1998. Based on the long observation period, there is a lack of moderate magnitude earthquake ($M_L \geq 5$) in this area before the 1998 event. Moderate magnitude earthquakes shut off again after the occurrence of the 1998 event in the shelf periphery area. The maximum MM intensity produced by this event (VII MM) was designated to Ras El-Hikma which is located about 50 km from the event (Hassoup and Tealeb, 2000). Alexandria City experienced an intensity of V–VI. The 1998 earthquake was felt like a great distance as Nicosia, Cyprus with an Intensity of II-MM, according to information from the International Seismological Centre (ISC). The most recent event is the April 11, 2020 earthquake which originated along one of the WNW-ESE trending faults existing along the Egyptian coast.

4. Data and data analysis

In this study, we used three programs, which are included in Seisan software version 2.5 (Havskov 1999 & 2020). FOCMEC; HASH and PINV software are used to invert the polarity data for eleven earthquakes on the Egyptian continental margin to get the optimum focal mechanism solutions. The best fitting solution were computed using two different velocity models; WD and MC, which cover a variety of possible structures for the study area

(Marzouk & Makris, 1979). We also examine the impact of changing the source depth on the solutions. The depth inaccuracy will only affect the take-off angle, as is well known. For events that occurred after 1998, We compute the variation in take-off angle for a depth change of 1-km. The typical depth uncertainty in earthquake location for these events is 1-km. This small uncertainty is attributed to the installation of several local and regional stations after 1998. The typical depth uncertainty for events documented before 1999 is 5-kilometers. Therefore, we compute the variation in take-off angle of these events for a depth change of 5-km. In recent years, the perfect coverage of the surrounding seismological networks for the recent events in addition to the availability of high-quality digital waveform data offers the opportunity to reduce the azimuth gap and get high-quality solutions.

The first-motion polarities of the P-waves are picked as a first step manually by careful investigation of the digital waveform data recorded by the Egyptian National Seismological Network and International Data Center of the comprehensive Test Ban Treaty Organization (CTBTO) in addition to the available polarities in the International Seismological Center (ISC). We used PINV software to produce a polarity-based initial fault plane solution which was intended to assist with other fault plane solution methods (Suetsugu, 1998). In PINV, polarities are treated as amplitudes of +1 and -1 identical to compression and dilation respectively. This is a vast generalization since there will be a wide variety of actual amplitudes through the focal sphere. Under the constraint of finding a single double couple solution, the data set of amplitudes is then inverted to get the moment tensor solution. The advantage of using this technique is that it provides the best estimate of the fault plane solution very rapidly, regardless of how simplified it is. We used PINV to obtain an idea about the preliminary solution. Unsurprisingly, PINV does not have an uncertainty error parameters estimate to recognize how accurate the solution it is.

Another commonly used software is FOCMEC. This software performs a grid search to find a variety of possible alternative solutions based on the selected number of polarity data errors. These solutions are estimated using a 3° grid search. We chose the favored one. The

298 HASH software (Hardebeck and Shearer, 2002, 2003), much like the FOCMEC program,
299 defines fault plane solutions from polarities of the P-waves first onset and amplitude ratios.
300 HASH produces solutions with less than a specified number of polarity errors and less than the
301 specific amplitude errors limit. If no solutions are found, error limits are increased and a large
302 number of solutions are usually reestablished. Using this technique, an approximation of the
303 best solution was generated and the probable errors are evaluated. The leading advantage of
304 HASH software is that it automatically explores one or a few of the best solutions, while for
305 FOCMEC, we must pick one out of many possible solutions. FOCMEC does not also provide
306 an estimation of the solution's errors while HASH determined uncertainty parameters in the
307 solution. Therefore, we will rely on the HASH program to evaluate solutions in this study.

308 The focal solutions from PINV, FOMEC and HASH software for these events are
309 plotted as shown in Figures 4 and Table 2. We calculated the uncertainty parameters, including
310 weighted fraction of polarity misfits, fault plane uncertainty, and station distribution ratio from
311 HASH software (Table 3) beside the azimuth and take-off angle gap. Then, we were able to
312 detect the quality factors for each event based on calculations of HASH uncertainty parameters.
313 For each event, a number of focal mechanism solutions were created, using take-off angles
314 estimated from a combination of velocity structure models and potential source depths. The
315 acceptable mechanisms for each trial were found using a grid search of 3° along strike, dip and
316 rake. The optimal solution is thus obtained by averaging the appropriate solutions after any
317 extremist solutions are removed. Consequently, the mechanism that is farthermost away from
318 the average is eliminated and then a new average is computed until all of the remaining
319 mechanisms are within 30 ° of the optimal solution. The range of the solutions is calculated by
320 the root-mean-square (RMS) angular difference between the agreeable mechanisms and the
321 optimal one.

322 The quality control factors have been assumed to dependent on the initial tests done
323 by Kilb & Hardebeck, 2006 for the best indicators to detect the best mechanism solutions from
324 the alphabetic letter ‘A’ as best sequent to letter ‘F’ for bad solutions. The station distribution

ratio (STDR) is a number that represents how data is distributed on the focal sphere relative to the radiation pattern (Reasenberg and Oppenheimer 1985). This ratio is < 0.5 when a large number of data lie near the nodal planes in the solution. Such a solution is less robust than the one for which STDR>0.5 and should be carefully examined before being rejected. According to Kilb & Hardebeck, 2005, the Root mean square error (RMS) of the fault plane uncertainty was considered as the best single parameter indicator of mechanism quality and was calculated according to the following equation: 0.5*(rms_diff(1)+rms_diff(2)), with values ≤ 35° indicating the best mechanisms. Another uncertainity parameter is the misfit function which is defined as the fraction of weighted misfit polarities, and therefore, a perfect fit to data corresponds to 0 percent (or 0.0) and an ideal misfit to 100 % (or 1.0). The number of impulsive polarities misfit is minimized due to the search algorithm which determines a group of acceptable nodal plane depending on the velocity earth structure and calculated takeoff angles (Lentas, 2017).

5. Results

Comparing the solutions from the three programs used in this study, we find that the majority of them agree with only minor differences in-plane directions and angles of dip, while a small number of them vary in dip directions of the planes. For the majority of solutions, FOMEC and HASH codes provide identical focal mechanism solutions. We address solutions derived from the HASH code in this study because it assesses uncertainties quantitatively. Due to this reason, this code is to be superior compared to the other ones. In general, the takeoff angles calculated using the various models employed in this study reveals discrepancies for only source depths of 11 and 19 km. For the source depth of 11 km, the differences in takeoff angles derived from the two models are within 14^{o}, while the depth of 14 km results in a difference of about 6 ^{o}. In this study, we designate quality factors for the eleven constructed focal mechanism solutions. About 90% percent of the solutions have higher qualities of grades

A and B, while the mechanism of the 1951 earthquake was given E quality grade due to the largest azimuthal gap (Table 3).

All available solutions in the Egyptian continental margin show that there are three main types of focal mechanism solutions. Pure reverse faulting mechanism (Events No.2 and 5, Table 2 and Figures 4&5), reverse faulting mechanism with some strike-slip motion (Events Nos., 3 and 4, Table 2 and Figures 4&5) and strike-slip mechanism with some reverse dip-slip component (6,7, 9 and 10, Table 2 and Figures 4&5). Only one event of the first type (Event 2) is located in the western Nile cone province with two planes trending ENE and dipping towards SE and NW respectively. In the same province, there are only two events of the second type (Events 3 and 4). The first one gives fault planes striking in the NNW and ENE directions and dipping WSW and SSE respectively while the second one shows fault planes oriented NNE and ENE and dipping towards NNE and SW respectively. The last event of the first type (Event No.5) is located very close to the continental shelf periphery with two planes striking NNW-SSE and dipping towards NE and SW respectively.

The focal solutions of the third type are located in the central and eastern Provinces. The solutions of the third family (6, 7, 9 and 10, Table 2 and Figures 4&5) are similar with two planes trending NNW-SSE and NNE-SSW and dipping SE and NE or SW respectively. The fault plane solution of the events, which are located in the central, and the Eastern Provinces of the deep-sea fan demonstrate mainly strike-slip motion with some reverse component for the some events (Figures 4&5, Table 2). Although event 1 (Figures 4&5, Tables 2&3) shows a low-quality solution, we investigate its focal mechanism solution because it provides information that leads to the identification of the predominant fault type in the central zone outlimit of the Levantine basin. An extensional mechanism with two planes oriented ESE and NNW and dipping NNE and WSW respectively characterizes this event.

Two earthquakes with local magnitudes of M_L 4.3 and 3.8 occurred in 2015 and 2020 to the south of the Egyptian continental shelf (Events 8,11; Figures 4&5, Table 2). The two

377 focal mechanism solutions of both events reflect a normal faulting mechanism with a slight
378 strike-slip component. The solution of the first event consists of two planes trending ENE-
379 WSW and NNW-SSE respectively while the second event nodal planes strike to NNE and
380 NNW respectively.

381 The occurrence of six moderate magnitude earthquakes in the last 10 years
382 (Figures 4 & 5, Table 2) has enabled us to examine the main movements in the Egyptian
383 continental margin comparable to the tectonic regime. We compared the stress distribution in
384 the Egyptian continental margin zone obtained from the focal mechanism solutions with the
385 integrated stress distribution estimated by Tingey et al., 2012 from both drilling-
386 induced fractures and borehole breakouts and the stress pattern obtained from the GPS velocity
387 vectors (Zeman et al., 2010) as shown in Figure 6.

388

389 ## 6. DISCUSSIONS
390

391 We construct the focal mechanism solutions of moderate magnitude earthquakes
392 which occurred in the Egyptian continental margin during the period from 1951 to 2020 using
393 PINV, HASH, FOCMEC codes included inside Seisan software version 2.5 (Havskov 1999 &
394 2020). The main target is to evaluate these solutions in terms of their uncertainties especially
395 for earthquakes reported by a limited number of available stations prior to 2000, using HASH
396 software, which is characterized by its ability to measure uncertainties in quantitative way. It
397 should be noted that the previous studies of the focal mechanism solutions in the Egyptian
398 continental margin did not provide a quality control inspection. The second target was to
399 understand the tectonic regime of the Egyptian continental margin in the light of new seismic
400 activity occurring in the last years.

401 The earthquakes of January 30, 1951, of M_L5.6 and September 12, 1955, of M_L
402 6.2 are the largest and oldest earthquakes to hit the Levantine basin and the western province,

403 respectively. The focal solutions of these events manifest normal fault with slight strike-slip
404 component and reverse fault mechanism respectively. The first solution coincides with the
405 results of the previous studies (Constantinescu et al., 1966 and Korrat et al., 2005). The
406 solutions of Constantinescu et al., 1966 and Korrat et al., 2005 for the second event gave the
407 same type of mechanism with only changes in both plane and dip direction, as well as the
408 presence of small strike slip component. The focal mechanism solutions presented here for the
409 events of June 09, 1988, and May 28, 1998, which occurred in the western province and shelf
410 periphery area respectively show quality A reverse faulting mechanism with some strike-slip
411 component. The solutions of Korrat et al., 2005, Abou Elenean, and Hussein, 2007 for these
412 events demonstrated the same mechanisms with a slight change in the fault parameters. The
413 earthquake of April 09, 1987, which occurred in the western province as well, demonstrates a
414 quality B reverse faulting mechanism with some strike-slip component. This solution
415 completely opposes the solutions of Korrat et al., 2005 that shows pure normal faulting. The
416 direction of stress at **Western Province** is inconsistent with the NNE-SSW compression
417 direction achieved by Tingay et al., 2012 from drilling-induced Fractures and borehole
418 breakouts in the same zone (Figure 6). This mismatch implies that deformation in this area is
419 not consistent at both the surface and the depth. It also fits the direction of the compressional
420 axis deduced from the analysis of the Egyptian GPS permanent stations (Zeman et al., 2010)
421 and the relative direction of Nubia plate motion with respect to Eurasia (Reilinger et al., 2006).

422 In the central province, the October 12, 2012, and January 17, 2013 earthquakes were
423 occurred. Many authors have been interested in these two events with giving different
424 solutions. The solutions of Badawy et al., 2015 extracted from the moment tensor inversion of
425 some local stations from the Egyptian National Seismological Network demonstrated a normal
426 faulting mechanism with a slightly strike component for both events. On the other hand, the
427 focal mechanism solution of October 19, 2012, constructed by Hassoup et al., 2016 from both
428 local and regional stations using FOCMEC, suggested a reverse faulting mechanism with a
429 significant strike-slip component. The focal mechanism solutions estimated by PMAN

430 software of Suetsugu, 1998 for the October 12, 2012, and January 17, 2013 earthquakes
431 showed strike-slip motion with reverse component (Badreldein et al., 2018) Uncertainties
432 associated with solutions for both events are not evaluated by the different author. Our A-
433 quality solutions which agree with the solutions of Badreldein et al., 2018 are distinguished
434 by an evaluation of uncertainties. In our analysis, we also used more stations from local and
435 regional distances with a smaller azimuth gap compared to the solutions of the previous works.
436 These focal mechanism solutions in the central Nile cone province are located along the NE-
437 SW trending faults which are located within the Rosetta-Qattara fault zone. The plane trending
438 NE-SW is related to the trend of faults in this zone and shows an oblique right-lateral strike-
439 slip with a reverse component. The same sense of motion appeared to be present during the
440 Early Miocene along the same fault (Hanafy et al., 2017). The eastern Nile Delta Kattanyia
441 fault, which is subparallel to the Rosetta-Qattara fault zone, reflects the same sense of motion.
442 Alamein fault, which is considered an inland extension of the Qattara-Rosetta fault,
443 experienced an earthquake with normal dip-slip motion (Figure 5).

444 The mechanism of the earthquake which happened in 19980528 (event 5 in Table 2
445 and Figure 5) that occurred near the continental shelf periphery shows a northeast rotation of
446 the compressional axis, in good agreement with the stress pattern calculated by Zeman et al.,
447 2010 (Figure 6). The occurrence of the reverse faulting mechanism may be attributed to the
448 far-field effect of the SSW oriented Hellenic arc velocity vectors. This motion resulted from
449 the counterclockwise rotation of the velocity field in the eastern Mediterranean from the NW-
450 ward orientation towards the western part of the Egyptian continental margin with a significant
451 increase in vector magnitude (Reilinger et al., 2010, Cavazza et al., 2004). The major normal
452 fault that bounds the Alamein extensional basin from its northwestern side (Moustafa,
453 2020) coincides with the fault plane trending ENE. The same sense of motion was also found
454 along with one of the WNW-ESE trending coastal faults. The presence of such types of
455 motions on Egyptian territory reflects a change in the stress field to the dominant extensional
456 field.

7. CONCLUSIONS

Continental margins usually do not show plain, linear geometries. Consequently, a very complicated pattern of deformation occurs when they are involved in the collision process (Bosworth, 2014). The spatial distribution of the focal mechanism solutions in the Egyptian continental margin showed two deformation zones, the western province zone and the eastern-central provinces zone. The fault plane solution in the western province zone of the Nile Deep-Sea Fan shows margin perpendicular NNW-SSE compression direction, which generates a reverse faulting mechanism with some strike-slip motion. The mechanism of the earthquake that occurred near the continental shelf periphery shows a northeast rotation of the compressional axis, in good agreement with the stress pattern calculated by Zeman et al., 2010. The occurrence of the reverse faulting mechanism may be attributed to the far-field effect of the SSW oriented Hellenic arc velocity vectors. This motion resulted from the counterclockwise rotation of the velocity field in the eastern Mediterranean from the NW-ward orientation towards the western part of the Egyptian continental margin with a significant increase in vector magnitude (Reilinger et al., 2010, Cavazza et al., 2004).

The structural pattern in the eastern-central province zone is a product of dynamic interaction between two major fault trends; the NE-SW trending Rosetta-Qattara fault zone and the NW-SE trending Misfaq-Bardawil Shear Zone. Within the present day stress regime, these two main fault trends are very likely active, but they have been displayed little noticeable activity for a long period. In the future, these faults could lead to damaging earthquakes. These two conjugate fault trends accommodate the active deformation in this province. The presence of earthquakes along the Rosetta-Qattara fault zone indicates that they are related to the reactivation of an old fault zone that was formed during the Neo-Tethyan rifting phase. The maximum horizontal stress S_{hmax} estimated from both drilling-induced fractures and borehole breakouts (Tingay et al., 2012) in this zone is in good agreement with the P-axis calculated from the solutions in this zone. This consistency is an indicator of surface and depth uniformity

484 of deformation. The maximum horizontal stress S_{hmax} in this province shows a complexity,
485 whereas the obtained WNW-ESE trending compressional stress axis is different from the N-S
486 direction of the plate convergent. There is also a change in the type of mechanism from nearly
487 pure reverse in the western part of the Nile cone to strike-slip with some reverse component in
488 central-eastern part. These disparities in the compressional stress direction and type of
489 mechanism may be related to the Eratosthenes Seamount which is an obstacle to the
490 subduction of the northern edge of the African plate below Cyprus at the central part of the
491 Cypriot arc. The central segment of the Cypriot arc showed not only N-S compressional
492 direction but also some shear movement (Kempler, 1998). This component of shear is related
493 to the sideway transfer of the crustal blocks as it encounters the Eratosthenes Seamount. The
494 internal deformation within the region of the Seamount block may also control the deformation
495 kinematics within the eastern-central provinces zone. In the central part of the Levantine Basin,
496 the type of mechanism changes to a normal dip-slip movement compared to the eastern-central
497 provinces zone which manifest strike-slip motion with some reverse component. The stress
498 pattern observed by Ghalayini et al., 2014, which was based on a three-dimensional seismic
499 reflection survey, agrees well with the estimated NE-SW extensional regime in this study. In
500 this part of the basin, this survey revealed the presence of orderly distributed NW-SE striking
501 normal faults.

502 There is only available single focal mechanism solution in the eastern province, which
503 is similar to the solutions existing in the central province. This solution is located along an
504 NNW-SSE trending fault in the sub-linear Misfaq-Bardawil Shear Zone. We believe that the
505 NNW-SSE trending plane of the focal mechanism solution represents the actual fault plane.
506 This fault plane shows a sinistral strike-slip sense of motion with a minor reverse component,
507 This sense of motion reflects higher consistency with the one inferred by El Barkooky and
508 Helal.,2002.

509

510

Data availability. All used data and related results of this article are presented in the paper.

Author contributions. All authors have been prepared the manuscript, AS, HH and ME collected and analyzed the seismicity and focal mechanism data and AS, ME and MA prepared and analyzed the focal and stress distribution maps, all authors participated to the interpretations, discussions, and revision of the manuscript.

Acknowledgements. We are grateful to the Egyptian National Seismological Network and the International Data Center of the Comprehensive Test Ban Treaty Organization and the International Seismological Centre (ISC) for providing the seismological data.

This research did not receive any specific grant from funding agencies in the public, commercial, or not-for-profit sectors

References

Argyriadis I. , De Graciansky P.C. , Marcoux J. and Ricou L.E. (1980). the opening of the Mesozoic Tethys between Eurasia and Arabia-Africa 26e Congruous Geology. International, Paris, Colloq. C5, 199-214.

Abdel Aal, A.; Day, R. and Lelek, J. (1992). Structural evolution and styles of the northern Sinai, Egypt. 11th Exploration & Production Conference, Egyptian General Petroleum Corporation, Cairo, Egypt, 547-562.

Abdel Aal, A., El Barkooky, A., Gerrits, A., Meyer, H., Schwander, M. and Zaki, H. (2000). Tectonic evolution of the Eastern Mediterranean Basin and its significance for hydrocarbon prospectively in the ultra-Deepwater of the Nile Delta. The Leading Edge, pp. 1086-1102.

Abdel Aal A., EL Barkooky, A., Gerrits, M., Meyer, H., Schwander, M. and Zaki, H. (2001). Tectonic evolution of the Eastern Mediterranean Basin and its significance for the hydrocarbon prospectively of the Nile Delta Deepwater area, GeoArabia, 6, 363-384.

Abou Elenean, K.M. (1997). Seismotectonics of Egypt in relation to the Mediterranean and Red Sea tectonics. (Doctoral dissertation), Retrieved from Fac. Sci. Ain Shams Univ., Egypt.

Abou Elenean, K.M., Hussein, H.M. (2007). Source mechanism and source parameters of May 28, 1998 earthquake, Egypt. Journal of Seismology, 11, 259–274. https://doi.org/10.1007/s10950-007-9051-5

Abd EL Fattah, B.K., Yousef, M. and Moustafa, A.R. (2018). 2D structural restoration of the Rosetta fault system, offshore western Nile Delta, Mediterranean basin, Egypt, Journal Applied Geophysics, 17, 83-98.

Argus, D. F., Gordon, R. G., DeMets, C. and Stein S. (1989). Closure of the Africa-Eurasia-North America plate motion circuit and tectonics of the Gloria fault, Journal of Geophysical Res., 94, 5585–5602. ISSN: 0148-0227.

Barrier E., N. Chamot-Rooke and G. Giordano (2004)**.** Geodynamic Maps of the Mediterranean – sheet 1 : Tectonics and kinematics, Commission for the Geological Map of the World (CGMW) & Unesco, 1 sheet : 99x53 cm, 1:13.000.000 scale. Retrieved from https://maps.princeton.edu/catalog/princeton-kh04dr520

Badreldin H., Abd el-aal A.K, Toni M. and El-Faragawy K. (2018). Moment tensor inversion of small-to-moderate size local earthquakes in Egypt, Journal of African Earth Sciences, 151, 153-172. DOI: 10.1016/j.jafrearsci.2018.12.004.

Badawy, A., Mohamed, G., Omar, K. and Faried, W. (2015). The northern Egyptian continental margin, Journal of African sciences, 101, 177-185. http://dx.doi.org/10.1016/j.jafrearsci.2014.09.009.

Bondár, I. and D.A. Storchak (2011). Improved location procedures at the International Seismological Centre, Geophysical Journal International, 186, 1220-1244, doi: 10.1111/j.1365-246X.2011.05107.x.

Bosworth, W., Khalil, S., Clare, A., Comisky, J., Abdelal, H., Reed, T. and Kokkoros, G. (2014). Integration of outcrop and subsurface data during the development of a naturally fractured Eocene carbonate reservoir at the East Ras Budran concession, Gulf of Suez, Egypt. Geological Society, London, Special Publications, 374, 333-359. https://doi.org/10.1144/SP374.3.

Bosworth, W. (2008). North Africa-Mediterranean present-day stress field transition and implications for fractured reservoir production in the eastern Libya basins, Geology of East Libya, 4, 123–138.

Cavazza,W., Roure, F.M., Spakman,W., Stampfli, G.M. and Ziegler, P.A. (2004). The TRANSMED Atlas. The Mediterranean region from crust to mantle geological and geophysical framework. A Publication of the Mediterranean Consortium for the 32nd International Geological Congress 2004, XXIV, 141, 44).

Constantinescu, L., Ruprechtova, L. and Enescu, D. (1966). Mediterranean-Alpine earthquake mechanisms and their seismotectonic implications. Geophysical Journal International, 10 (4), 347-368.

Dolson, J. C., M. Atta, D. Blanchard, A. Sehim, J. Villinski, T. Loutit and K. Romine (2014). Egypt's future petroleum resources: A revised look into the 21st century, *in* L. Marlow,

C. Kendall and L. Yose, eds., Petroleum systems of the Tethyan region: AAPG Memoir, 106, 143–178.

Eyal, Y. and Reches, Z. (1983). Tectonics analysis of the Dead Sea rift region since late – Cretaceous based on Mesostructures, Tectonics, 2, 167-185. **https://doi.org/10.1029/TC002i002p00167**.

Freund, R. , Garfunkel Z., Zak I., Goldberg M., Weissbrod T., Derin B., Bender F., Wellings F. E. and Girdler R. W. (1970). The Shear along the Dead Sea Rift [and Discussion]." Philosophical Transactions of the Royal Society of London. Series A, Mathematical and Physical Sciences, 267(1181), 107–130. Retrieved from www.jstor.org/stable/73612.

Ghalayini, R., J.-M. Daniel, C. Homberg, F. H. Nader, and J. E. Comstock (2014), Impact of Cenozoic strike-slip tectonics on the evolution of the northern Levant Basin (offshore Lebanon), Tectonics , Vol. 33, pp.2121– 2142, doi:10.1002/2014TC003574.

Garfunkel, Z. (1981). Internal structure of the Dead Sea leaky transform (rift) in relation to plate kinematics, Tectonophysics, 80, 81–108.

GEBCO (update 2019). Digital Atlas published by the British Oceanographic Data Centre on behalf of IOC and IHO, Bathymetry data 15 arcs second.

Hussein, H.M., Abou Elenean, K.M., Marzouk, I.A., Korrat, I.M., Abu El-Nader, I.F., Ghazala, H. and ElGabry, M.N. (2013). Present-day tectonic stress regime in Egypt and surrounding area based on inversion of earthquake focal mechanisms: Journal of African Earth Sciences, 81, 1–15, doi: 10.1016/j.jafrearsci.2012.12.002.

Hardebeck, J. L. and P. M. Shearer (2002). A new method for determining first-motion focal mechanisms, Bull. Seism. Soc. Am., 92, 2264-2276.

Hassoup, A., Toni, M., Farag, S., M., Helal, A. M. and Mohamed, E., K. (2016). Source mechanism and parameters of the 19 October 2012 earthquake, northern Egyptian continental margin, Arabian Journal of Geosciences, 9:313, DOI: 10.1007/s12517-016-2338-5.

Hanafy, S., Nimmagadda, S.L., Mahmoud, S.E. and Mabrouk W.M. (2017). New insights on structure and stratigraphic interpretation for assessing the hydrocarbon potentiality of the offshore Nile Delta basin, Egypt. Journal Petroleum Exploration Production Technology **7,** 317–339 , https://doi.org/10.1007/s13202-016-0264-4.

Hassoup, A. and Tealeb, A., (2000). Attenuation of intensity in the northern part of Egypt associated with the May 28, 1998 Mediterranean earthquake. Acta Geophysica Polonica, 48, 79-92.

Havskov, J., Voss, P.H. and Ottemoller, L. (2020). Seismological Observatory Software: 30 Yr of SEISAN. Seismological Research Letters, 91 (3): 1846-1852. DOI: https://doi.org/10.1785/0220190313 .

615 **Hengesh, J.V. and Whitney, B.B.** (2016). Transcurrent reactivation of Australia's western
616 passive margin: An example of intraplate deformation from the central Indo-Australian plate.
617 Tectonics, 35 (5), 1066-1089.
618 **Hardebeck, J. L., & Shearer, P. M.** (2008). HASH: A FORTRAN Program for Computing
619 Earthquake First-Motion Focal Mechanisms–v1. 2–January 31, 2008.
620 **Johnston, Arch C. (1989).** The seismicity of stable continental interiors. , In S. Gregersen,
621 and P. W. Basham (Eds.), Earthquakes at North-Atlantic Passive Margins Neotectonics and
622 Postglacial Rebound. Kluwer Academic Publishers, 1-716, Dordrecht / Boston / London.
623 **Korrat, I.M., El Agami, N.L., Hussein, H.M., and El-Gabry, M.N.** (2005). Seismotectonics
624 of the passive continental margin of Egypt, Journal of African Earth Sciences 41. 145–150.
625 DOI: 10.1016/j.jafrearsci.2005.02.003.
626 **Havskov, J., and Ottemoller, L.** (1999) Seisan Earthquake Analysis Software. *Seismological*
627 *Research Letters* ;; 70 (5): 532–534. doi: https://doi.org/10.1785/gssrl.70.5.532.
628 **Kreemer C., Chamot-Rooke N.** (2004). Contemporary kinematics of the southern Aegean
629 and the Mediterranean Ridge, international geophysical journal, 157, 1377-1392.
630 **Kempler, D.,** (1998). Eratosthenes Seamount: the possible spearhead of ancient continental
631 collision in the Eastern Mediterranean. In: Robertson, A.H.F., Emeis, K.C., Richter, C.
632 Camerlenghi, A. (Eds.), Proceedings of the Ocean Drilling Program. Scientific Results, 160,
633 709–721.
634 **Loncke, L., Gaullier, V., Mascle, J., Vendeville,B. and Camera, L.** (2006). The Nile deep-
635 sea fan: an example of interacting sedimentation, salt tectonics, and inherited subsalt
636 paleotopographic features. Marine and Petroleum Geology, 23, 297–315.
637 DOI: 10.1016/j.marpetgeo.2006.01.001.
638 **Le Pichon, X., Gaulier, J.-M.** (1988). The rotation of Arabia and the Levant fault system.
639 Tectonophysics 153, 271–294. https://doi.org/10.1016/0040-1951(88)90020-0.
640 **Lentas, K.** (2017). Towards routine determination of focal mechanisms obtained from first
641 motion P-wave arrivals, Geophysical Journal International, , 212(3), 1665–1686.
642 https://doi.org/10.1093/gji/ggx503.
643 **May P.R.** (1991). The Eastern Mediterranean Mesozoic basin: evolution and oil habitat,
644 AAPG Bulletin, 75, 1215-32. DOI:10.1306/0C9B2911-1710-11D7-8645000102C1865D.
645 **Mascle, J., & Tiphaine, Z., & Bellaiche, G., & Droz, L. & Gaullier, V., & Loncke, L., &**
646 **Science Party.** (2001). The Nile deep sea fan: Preliminary results from a swath bathymetry
647 survey. Marine and Petroleum Geology, 18, 471-477. 10.1016/s0264-8172(00)00072-6.
648 **Maamoun, M., Megahed, A. and Allam, A.** (1984). Seismicity of Egypt: NRIAG Bulletin,
649 IV(B), 109–160.

650 **Moustafa, A.R. (2020).** Mesozoic-Cenozoic Deformation History of Egypt**. In Hammi, Z.,**
651 **EL-Barkooky A., Martinez Frias, J., Fritz, H. and Abd EL-Rahman, Y. (Eds.).** The
652 geology of Egypt, regional geology reviews. Springer (1-726).
653 **Moustafa, A.R. and Khalil, M.H.** (1989): North Sinai structures and tectonic evolution
654 M.E.R.C. Ain Shams University Earth Sciences Series, 3, 215-231.
655 **Moustafa, A. and Khalil, M.** (1994). Rejuvenation of the eastern Mediterranean passive
656 continental margin in northern and central Sinai; new data from the Themed Fault, Geological
657 Magazine, (131), 435-448. DOI: https://doi.org/10.1017/S0016756800012085.
658 **Mcclusky, S., Balassanian, S., Barka, A., Demir, C., Ergintav, S., Georgiev, I., Gurkan,**
659 **O., Hamburger, M., Hurst, K., Kahle, H., Kastens, K., Kekelidze, G. and King, R.,**
660 **Kotzev, V.,** (2000). Global Positioning System constraints on plate kinematics and dynamics
661 in the eastern Mediterranean and Caucasus, Journal of Geophysical Research, 105, 5695–5719.
662 DOI:10.1029/1999JB900351.
663 **Kilb, D. and J. L. Hardebeck (2006).** Fault Parameter Constraints Using Relocated
664 Earthquakes: Validation of First Motion Focal Mechanism Data, Bulletin of the seismological
665 Society of America., 96 (3), 1140- 1158. doi: 10.1785/0120040239.
666 **Mcclusky, S., Reilinger R.,Mahmoud S., Ben Sari D. and Tealeb** (2003). GPS constraints
667 on Africa (Nubia) and Arabia plate motion, International geophysics Journal, 155, 126–138,
668 doi: 10.1046/j.1365246X.2003.02023.x .
669 **Mandal, P., A. Mangik, and R.N. Singh (1997).** Intraplate stress distribution induced by
670 topography and crustal density heterogeneities beneath the Killari, India, region, Journal of
671 Geophysical Research,102 (11), 719-729. https://doi.org/10.1029/96JB03627.
672 **Mosconi, A., Rebora, A.,Venturino. G., Bocc, P. and Khalil, M.** (1996) Egypt-Nile Delta
673 and North Sinai Cenozoic tectonic evolutionary model: a proposal. Proceeding of the 13th
674 Egypt General Petroleum Cooperation: Exploration and Production Conference, Cairo, Egypt,
675 Vol. I, pp. 203–224.
676 **Marzouk I., Makris J., (1990).** Deep seismic profiles in Egypt. Bulletin of the International
677 Institute of Seismology and Earthquake Engineering. 24, 1-40.
678 **Orwig R.O**. (1982). Tectonic framework of Northern Egypt and the Eastern Mediterranean
679 region, 6th exploration and production conference, Vol. 1, p 193–202.
680 **Quennell, A. M**. (1984), The Western Arabia rift system, in The Geological Evolution of the
681 Eastern Mediterranean, edited by J. E. Dixon and A. H. F. Robertson, Geology Society
682 London Spec. Publication, 17, 775–788.
683 **Reilinger, R.E., McClusky, S., Paradissis, D., Ergintav, S. and Vernant, P**. (2010).
684 Geodetic constraints on the tectonic evolution of the Aegean region and strain accumulation
685 along the Hellenic subduction zone, Tectonophysics, 488(1):22-30,
686 DOI:10.1016/j.tecto.2009.05.027.

Reilinger, R., McClusky, S., Vernant, P., Lawrence, S., Ergintav, S., Cakmak, R., Ozener, H., Kadirov, F., Guliev, I., Stepanyan, R., Nadariya, M., Hahubia, G., Mahmoud, S., Sakr, K., et al., (2006). GPS constraints on continental deformation in the Africa-Arabia-Eurasia continental collision zone and implications for the dynamics of plate interactions: Journal of Geophysical Research: Solid Earth, 111, 1–26, doi: 10.1029/2005JB004051.

Robertson, A.H.F. and Dixon, J.E. (1984). Introduction: aspects of the geological evolution of the Eastern Mediterranean, Geological Society of London, Special Publications, 17 (1), 1-74.
https://doi.org/10.1144/GSL.SP.1984.017.01.02.

Rosenbaum G., Lister G. S., Duboz C. (2002) Relative motions of Africa, Iberia and Europe during Alpine orogeny, Tectonophysics, (359), 117–129. DOI: 10.1016/S0040-1951(02)00442-0.

Reasenberg, P., and D. Oppenheimer, FPFIT, FPPLOT, and FPPAGE (1985). FORTRAN computer programs for calculating and displaying earthquake fault-plane solutions, U.S. Geological Survey Report no. 85-739, 109, DOI: 10.3133/ofr85739. Retrieved from http://pubs.er.usgs.gov/publication/ofr85739.

Shaaban, F., Lutz, R., Littke, R., Bueker, C., and Odisho, K. (2006). Source-rock evaluation and basin modelling in NE Egypt (NE Nile Delta and northern Sinai): Journal of Petroleum Geology, 29 (2), 103–124, doi: 10.1111/j.1747-5457.2006.00103.x.

Shearer, P. M., Hardebeck, J. L., Astiz, L. and Richards-Dinger., K. B. (2003). Analysis of similar event clusters in aftershocks of the 1994 Northridge, California, earthquake, *J. Geophys. Res.*, 108, B1. DOI: 10.1029/2001JB000685.

Saleh, M., and Becker, M. (2015). New constraints on the Nubia-Sinai-Dead Sea fault crustal motion: Tectonophysics, 651, 79–98. DOI: 10.1016/j.tecto.2015.03.015.

Sehim A., Hussein M., Kasem A., Shaker A. and Swidan N. (2002). Structural architecture and tectonic synthesis, Rosetta Province, West Nile Delta, Mediterranean Egypt. In Mediterranean offshore conference, Alexandria, 18 PP.

Suetsugu, D. (1998). Practice on Source Mechanism, International Institute of Seismology and Earthquake Engineering (IISEE) Lecture Note, Tsukuba, Japan, 104 pp.

Snoke, J. A., Munsey, J. W., Teague, A. G., and Bollinger, G. A. (1984). A program for focal mechanism determination by combined use of polarity and SV-P amplitude ratio data. Earthquake notes, 55.

Tassy A., Crouzy E., Gorini C., Rubino J-L., Bouroullec J-L. and Sapin F. (2015). Egyptian Tethyan margin in the Mesozoic: Evolution of a mixed carbonate-siliciclastic shelf edge (from Western Desert to Sinai), Marine and Petroleum Geology, 68, Part A, 565-581. DOI: 10.1016/j.marpetgeo.2015.10.011.

Tari, G., Hussein. H., Novotny, B., Hannke, K. and Kohazy, R. (2012) Play types of the deep-water Matruh and Herodotus basins, NW Egypt. Petroleum Geoscience,18, pp. 443–455. DOI: 10.1144/petgeo2012-011.

Tingay, M., Bentham, P., De Feyter, A. and Kellner, A. (2012). Evidence for non-Andersonian faulting above evaporites in the Nile Delta, Geological Society Special Publication, 367 (1), 155-170, DOI: 10.1144/SP367.11.

Zein El-Din M. Y., Hafez N.A. and Mahrous O. (2016). Application of fault seal Analysis, Buselli field, Onshore Nile Delta, Egypt, International Journal of Innovative Science, Engineering & Technology, 3 (1) , 369-375. ISSN 2348 – 7968.

Zeman, A., & Hassan, K., Holešovsk, J., Monem, A., Mohamed, S., Novotn, Z., & Mahmoud, Sa., Kostelecký, J., & Ali, R., (2010). Deformation between African and Eurasian Plate Estimated from the European and the Egyptian GPS Geodetic Networks. Acta Geodynamica et Geomaterialia,7, (1), 129-137.

741 Table 1 Summary of tectonic phases in northern Egypt and continental margin

ERA/ PERIOD		Epoch	AGE	Motion Continuity	Time in MY	Tectonic Phases	Tectonic movement Shape	Tectonic Results	Type/movement Direction	References
MESZOIC		Triassic	Lower Middle Upper	1	248	1.Theyan rift (Divergent movement between a from the Arabian and Eurasian plate)		Creation of extensional basins with NE-SW trending boundary fault in Northern Egypt and continental margin	Extension / NW–SE	Abdel Aal et al., 1992) Abdel Aal et al., 2001 Moustafa 2020
		Jurassic	Lower Middle Upper		206 180 159 144					
		Cretaceous	Lower Upper		112 65					
CENZOIC	PALEGENE	Palaeocene Eocene Oligocene		21	54.8 33.7 23.8	2.Convergence between the Afro-Arabian and Eurasian plates		Inversion of Tethyan extensional basin and reactivation of Rosetta fault (Western NDSF)	compression / ESE to SE and WNW direction	Orwig, 1982 Abdel Aal et al., 2001
	NEOGENE	Miocene Pliocene Pleistocene		3	20.8 5.3 1.8	3.Convergent between the Afro-Arabian and Eurasian plate (Eastern-Central Nile Deep-Sea Fan)		Positive inversion of Oligocene normal faults and reactivation of Misfaq - Bardawil shear zone (Eastern -central Nile Deep Sea Province)	compression / NE-SW direction due to local variation associated with the Eratosthenes Seamount	Mascle et al., 2001 Abdel Aal et al., 1992) Dolson et al., 2014
		Quaternary								

	Date	O.T			Lat.	Long.	Depth	Magnitude	Fault plane			P-axis		T-axis		Software used
									Strike	Dip	Rake	Trend	Plunge	Trend	Plunge	
1	19510130	23	07	27.66	32.3725	33.4537	15.0	5.7(MS)-5.6 (ML)	264.28	76.26	-165.33	127.56	20.00	37.44	00.34	FM
									285.5	86.00	-166.00	150.31	12.71	58.73	06.97	HASH
2	19550912	06	09	29.00	2.4183	29.7483	64.0	6.2 (MS)-6.2(ML)	275.90	65.40	101.01	375.65	19.68	206.77	67.73	FM
									193.00	59.00	84.00	287.00	13.01	87.00	67.00	PINV
									243.00	70.00	92.00	331.44	24.79	156.34	64.95	HASH
3	19870409	03	00	05.97	32.4493	29.0268	13.7	4.6 (mb) - 4.4 (ML)	170.94	73.23	47.85	290.75	17.33	38.87	44.91	FM
									162.47	79.64	42.86	286.01	20.24	32.08	36.89	HASH
4	19880609	02	18	23.93	32.1630	27.9509	06.0	4.9(mb)-4.5 (ML)	120.00	42.00	85.00	33.00	03.00	260.00	86.00	PINV
									277.18	60.50	151.66	148.60	03.21	241.30	39.82	FM
									289.70	57.90	146.00	164.08	02.34	256.44	45.29	HASH
5	19980528	18	33	31.93	31.4579	27.6242	27.0	5.5(mb)-5.9(ML)	125.00	30.0	94.00	31.54	14.99	204.85	74.87	FM
									120.00	42.00	85.00	33.00	03.00	260.00	86.00	PINV
									136.30	34.00	96.00	41.86	11.13	204.50	78.37	HASH
6	20121019	03	35	12.26	32.5770	30.9775	18.5	5.0(mb)-4.8 (ML)	139.55	70.00	01.45	096.26	12.92	002.73	14.96	FM
									137.00	77.00	-01.00	093.00	10.00	001.00	08.00	PINV
									138.46	75.01	00.00	93.99	10.55	02.01	10.55	HASH
7	20130117	21	17	35.07	32.0268	30.6421	11.5	4.8(mb)-4.5 (ML)	145.04	73.42	17.60	277.00	00.00	008.00	24.00	FM
									146.00	61.00	12.00	101.00	12.00	004.00	28.00	PINV
									144.7	71.5	23.27	275.32	02.33	06.62	29.28	HASH

									6	1						
8	20150903	01	44	40.54	30.6164	28.4589	15.6	4.5(mb)-4.3 (ML)	257.58	60.53	-151.67	113.48	39.79	206.15	03.20	FM
									269.00	70.00	-176	132.00	17.00	225.00	11.00	PINV
									260.0	68.00	-166.10	120.77	25.06	213.63	06.10	HASH
9	20190515	16	53	46.25	32.8060	32.6513	10.0	4.8 (mb)-4.0 (ML)	138.00	84.00	07.09	373.00	01.00	003.00	09.00	FM
									138.00	81.00	-11.00	094.00	15.00	185.00	01.00	PINV
									141.00	81.00	00.00	96.35	06.35	05.65	06.35	HASH
10	20190705	14	18	57.31	32.4875	30.8507	10.0	4.0 (mb)-4.1 (ML)	320.00	74.00	00.00	276.00	11.24	183.87	11.24	FM
									308.00	82.00	-14.00	283.0	16.00	354.00	04.00	PINV
									311.68	81.00	-02.02	267.00	07.77	176.51	04.95	HASH
11	20200411	16	30	58.81	31.5075	26.8042	10.0	3.9(mb)-3.8 (ML)	304.79	68.37	-145.00	165.96	39.27	070.69	06.41	FM
									303.00	80.00	-164.00	168.00	18.00	076.00	04.00	PINV
									302.90	66.00	-155.00	162.29	34.10	252.86	0.84	HASH

742

743 Table 2 Parameters of the focal mechanism's solutions located at the Egyptian continental margin using PINV, FOCMEC. HASH

Table 3 Uncertainties calculated from HASH software

Event NO.	Date	RMS Fault plane uncertainty	Weighted fraction of pol. misfits	Station distribution ratio	Azimuth gap	Takeoff angle gap	No. of polarities	Quality Degree According to Kilb &Hardebeck, 2005
	Y M D							
1	19510130	61.6	0.28	0.64	280	40	12	E
2	19550912	34.0	0.22	0.74	77	10	40	B
3	19870429	37.5	0.09	0.77	186	21	28	B
4	19880609	3.6	0.03	0.76	116	8	46	A
5	19980528	13.3	0.03	0.74	85	13	54	A
6	20121019	06.2	0.10	0.86	37	7	105	A
7	20130117	12.6	0.11	0.83	42	9	48	A
8	20150903	21.8	0.03	0.67	63	4	42	A
9	20190515	16.0	0.16	0.78	47	5	62	A
10	20190705	28.4	0.12	0.73	76	29	41	A
11	20200411	18.2	0.07	0.58	63	17	42	A

List of Figures

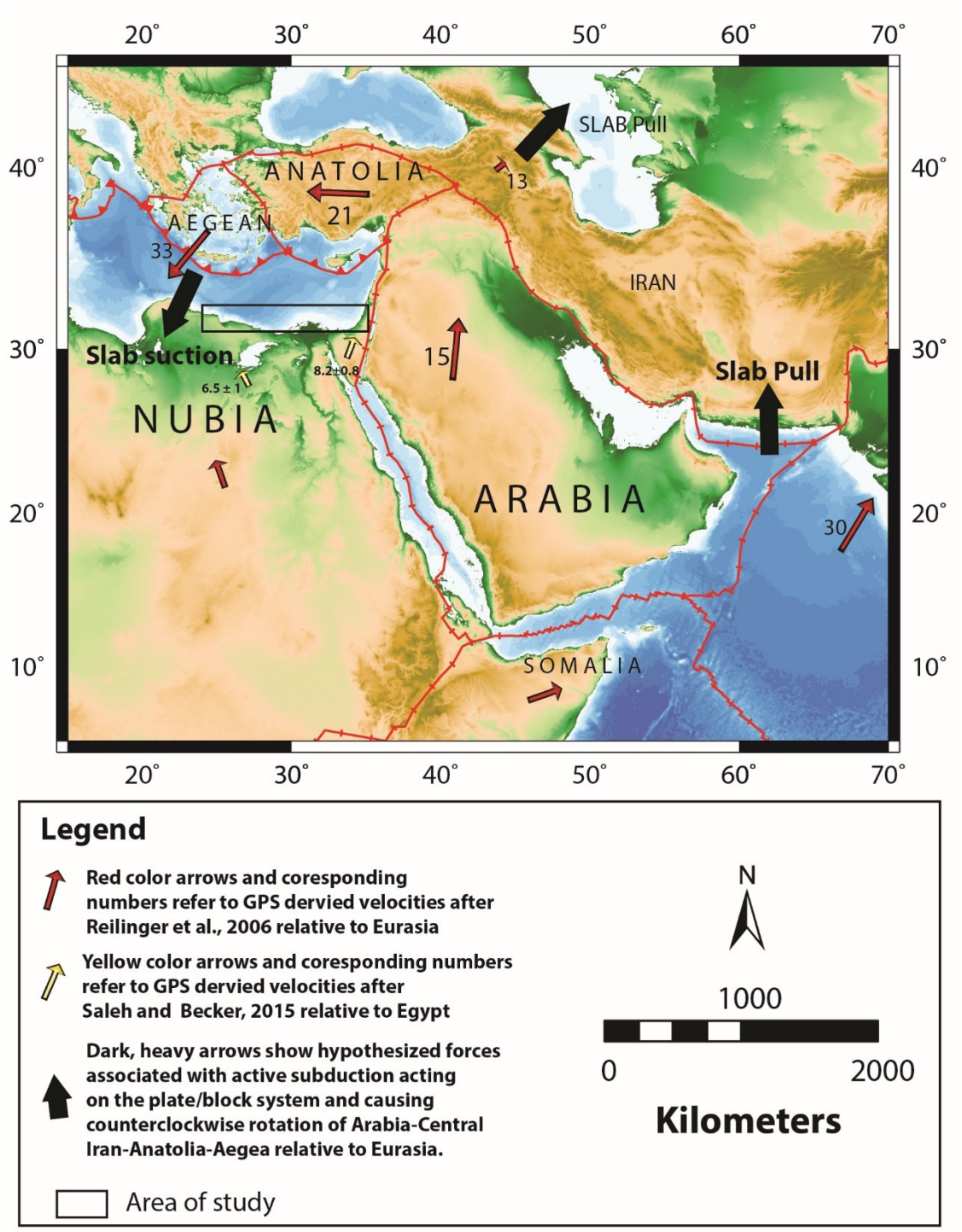

Figure 1. Arabia-Africa and Eurasia plates interaction and their influences on the Egyptian continental margin inferred from GPS derived velocities after Rellinger et al., 2006 & Saleh and Becker, 2015

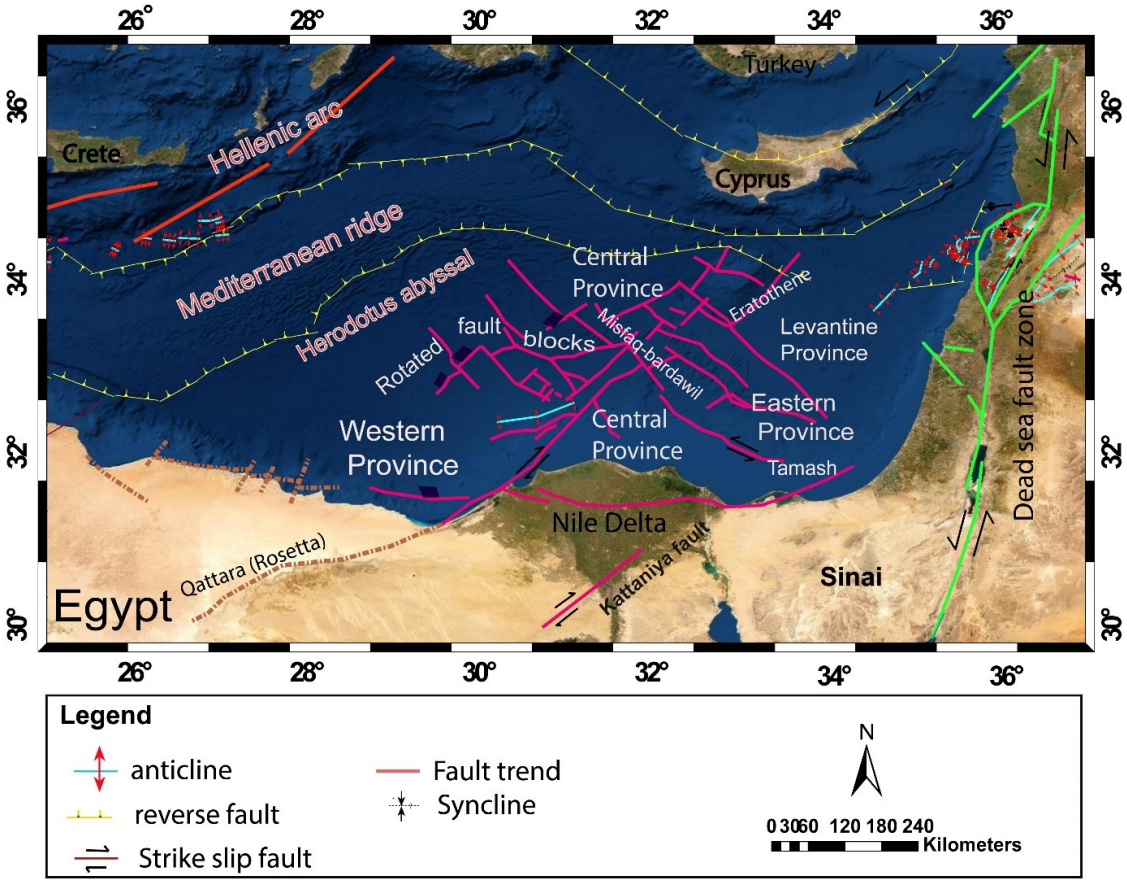

Figure 2. Tectonic structural elements along the Egyptian continental margin and adjacent areas in Eastern Mediterranean adopted from Abdel Aal, 2000 & 2001, Barrier et al., 2004, Loncke et al., 2006, Dilson et al., 2014, Ghalayini et al.,2014, Zein El-Din et al., 2016, Moustafa et al., 2020.

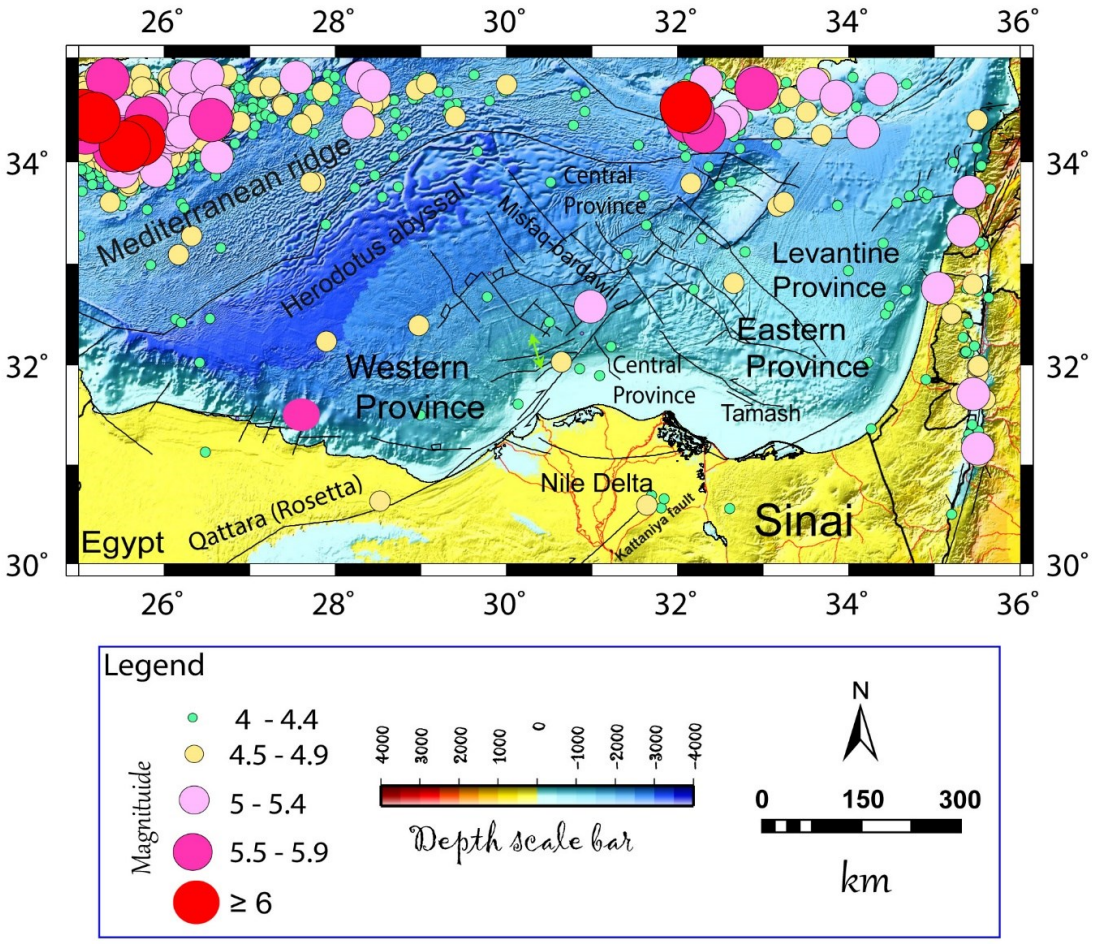

Figure 3. Seismicity of the Egyptian continental margin and the Eastern Mediterranean region ($3.8 \geq M_L \geq 6.0$).

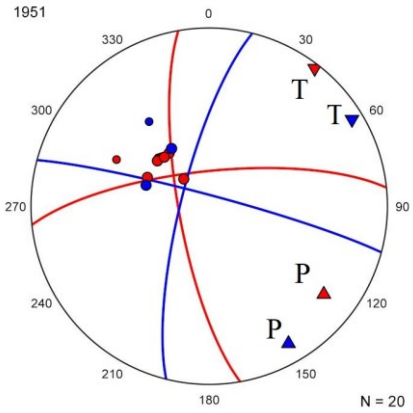

1. 19510130 earthquake mechanism (ML=5.6)

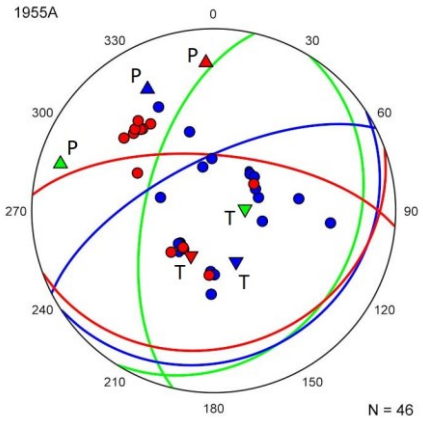

2. 19550912 earthquake mechanism (Ml=6.2)

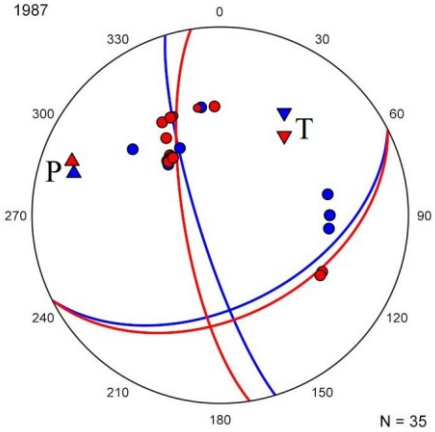

3. 19870429 earthquake mechanism (ML=4.4)

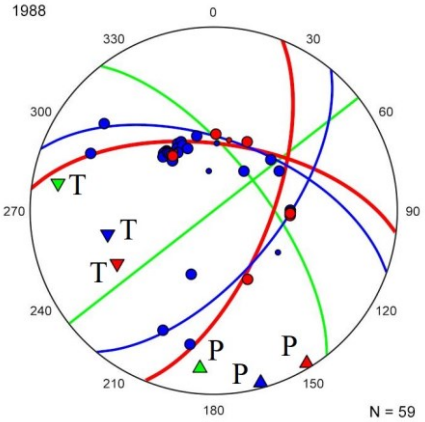

4. 19880609 earthquake mechanism (ML=4.5)

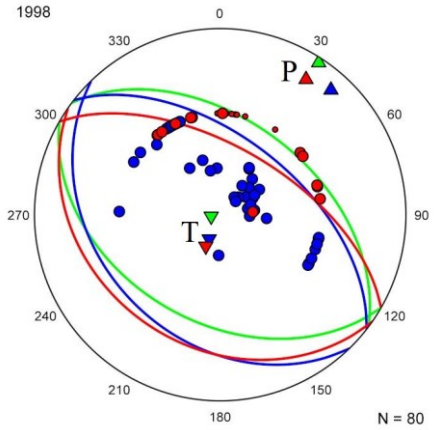

5. 19980528 earthquake mechanism (ML=5.9)

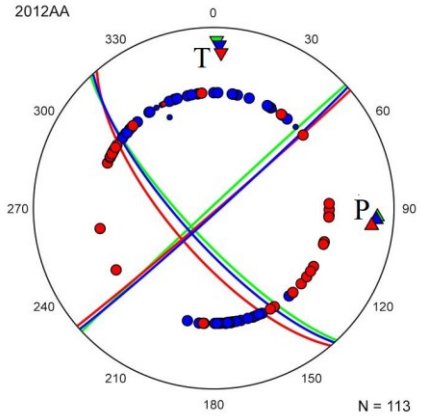

6. 20121019 earthquake mechanism (Ml=5.1)

788 Figure 4. The best fitted nodal planes for the polarity distribution of the constructed focal
789 mechanism solutions (Table 2); output from PINV as green colour, blue for FOCMEC, red for
790 HASH,.

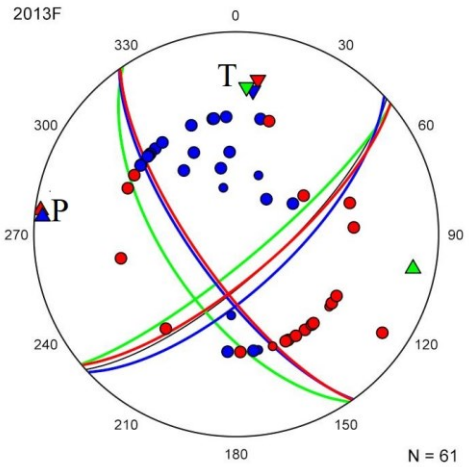

7. 20130117 earthquake mechanism (ML=4.8)

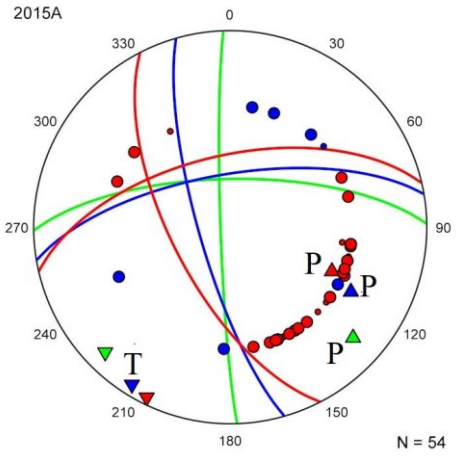

8. 20150903 earthquake mechanism (ML=4.2)

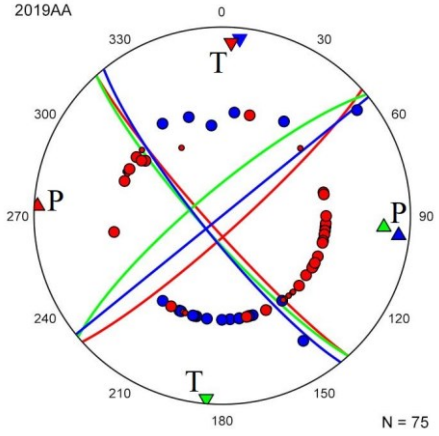

9. 20190515 earthquake mechanism (ML=5.1)

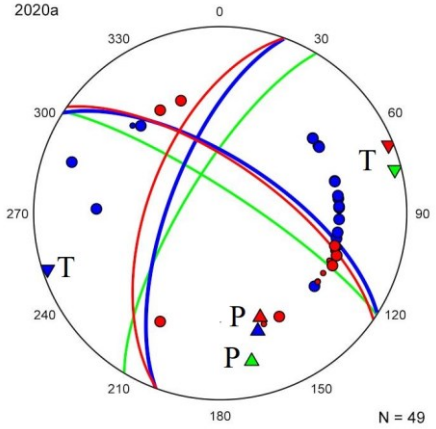

10. 20190705 earthquake mechanism (ML=4.8)

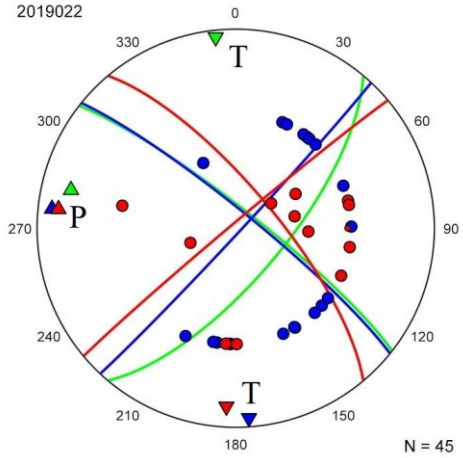

11. 20200411 earthquake mechanism (ML= 4.3)

791

792 Figure 4 continued

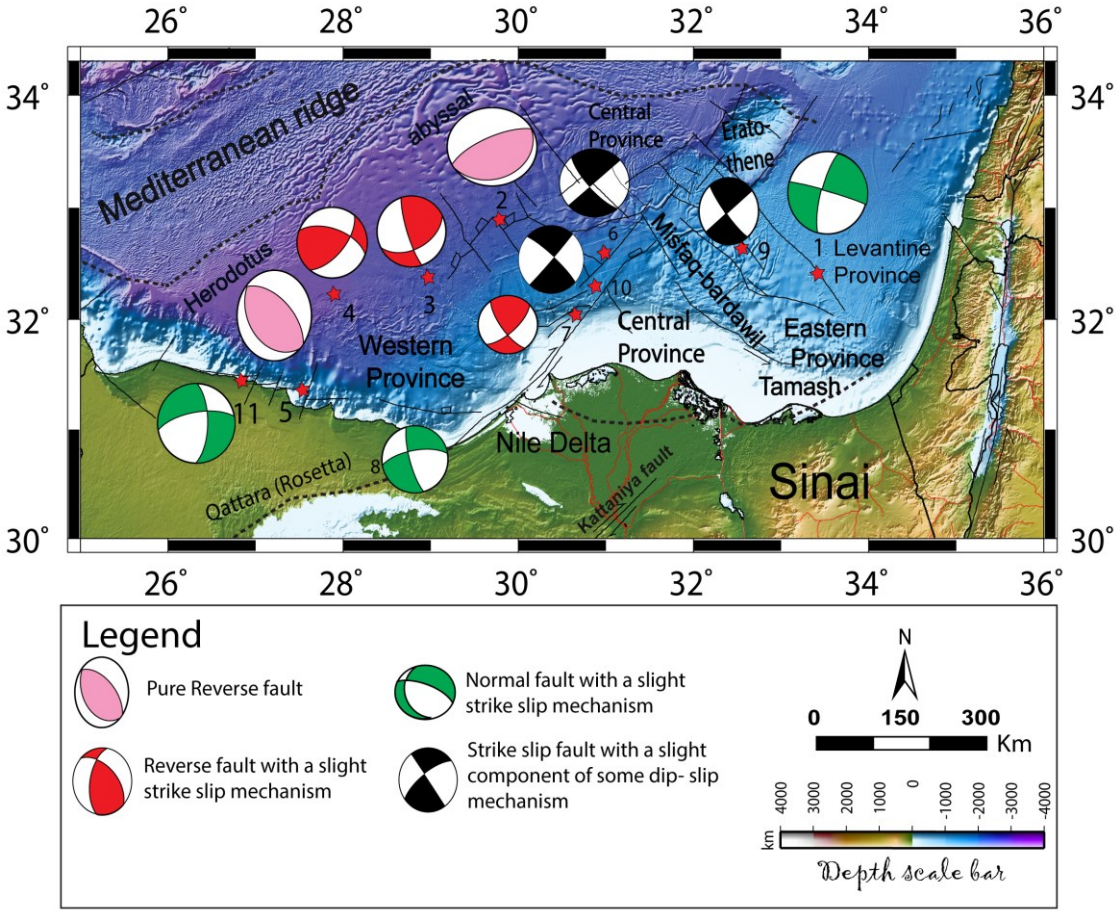

Figure 5. Focal mechanisms distributions calculated in this study using HASH software in the Egyptian continental margin.

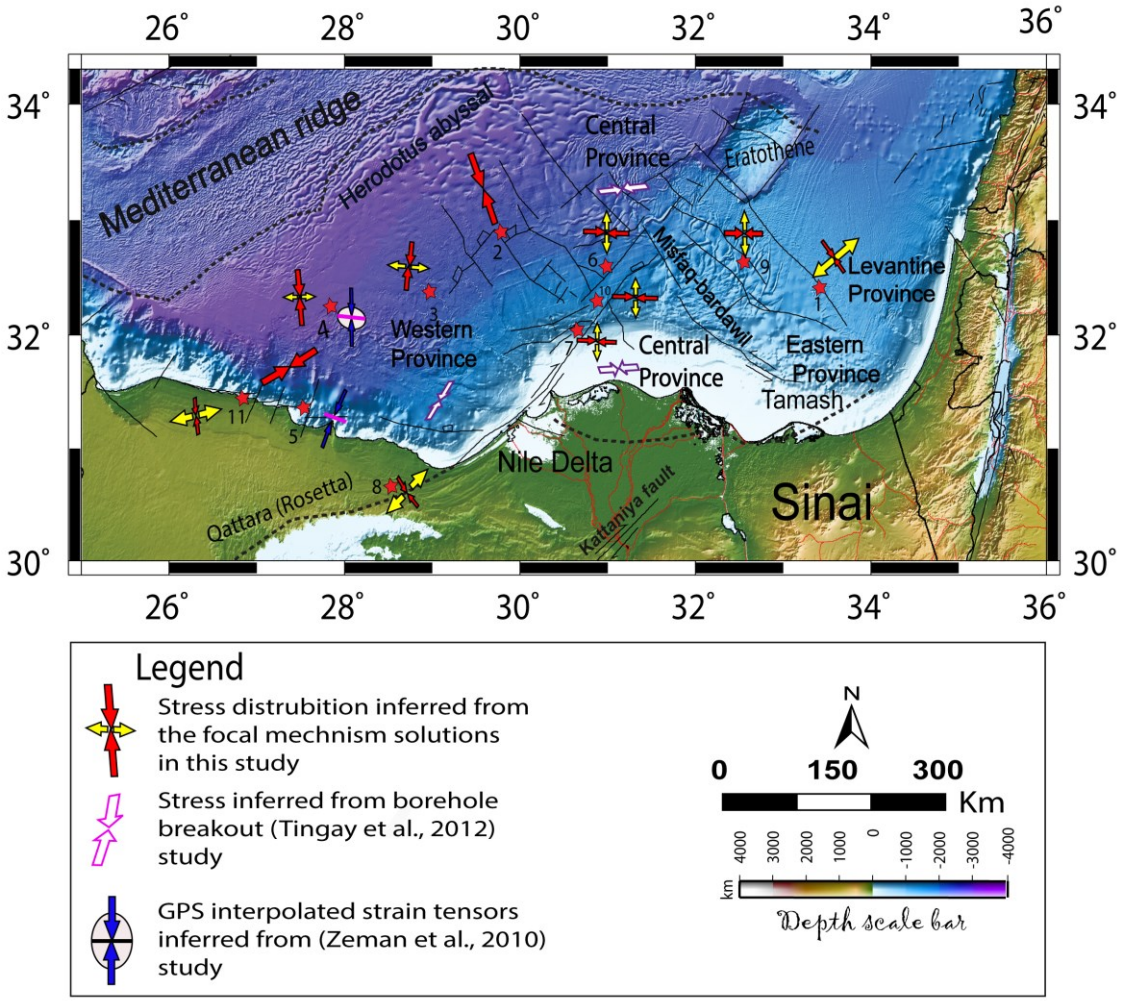

Figure 6. Stress distribution inferred from focal mechanisms in the Egyptian continental margin compared to the stress distribution obtained by Tingey et al., 2012 and strain tensor obtained from the work of Zeman et al.,2010.